Corrosion behavior in Hank`s solution of a magnesium-hydroxyapatite composite processed by high-pressure torsion

Debora Lopes[1]; Renata B. Soares[1]; Moara M. Castro[2]; Roberto B. Figueiredo[2,*];

Terence G. Langdon[3]; Vanessa F. C. Lins[1]

[1] Department of Chemical Engineering,
Universidade Federal de Minas Gerais, Belo Horizonte, MG 31270-901, Brazil
[2] Department of Metallurgical and Materials Engineering,
Universidade Federal de Minas Gerais, Belo Horizonte, MG 31270-901, Brazil
[3] Materials Research Group, Department of Mechanical Engineering, University of Southampton,
Southampton SO17 1BJ, U.K.

Abstract

It is known that magnesium (Mg)-hydroxyapatite (HA) composites can be produced by the room temperature consolidation of particles. The present study analyzes the corrosion behavior of an Mg-HA composite and makes a direct comparison with pure Mg. Samples of Mg-HA and of pure Mg were immersed in Hank`s solution for up to 60 hours and the microstructure and corrosion products were characterized by scanning and transmission electron microscopy and X-ray diffraction. Electrochemical tests were used to evaluate the corrosion behavior and a hydrogen evolution test was undertaken to determine the corrosion rate. The results show the corrosion rate of the Mg-HA composite is higher than for pure Mg but decreases significantly after ~10 hours of immersion in Hank`s solution. The increase in corrosion resistance of the composite is attributed to the formation of a protective layer of corrosion products with an external surface layer rich in Ca, P and O.

Keywords: high-pressure torsion; hydroxyapatite; magnesium; metal matrix composites; corrosion

*corresponding author: figueiredo@demet.ufmg.br / +55 31 34091925

1. Introduction

Magnesium and its alloys have a potential for use as temporary implants in medical applications. Since the metal does not passivate in physiological media, corrosion gradually removes matter which can be absorbed and then released by the body. It is generally accepted that magnesium is biocompatible and the release of relatively high amounts of the byproducts of its corrosion produces no significant toxicity [1]. Recent investigations [2]–[7] have shown that the processing of pure magnesium and its alloys by severe plastic deformation (SPD) techniques can improve the performance of these materials for medical applications due to the introduction of significant grain refinement and higher strength that increases the load-bearing capacity of the implant. Furthermore, some of these reports suggest that the grain refinement introduced by SPD can promote a more uniform corrosion and an enhanced corrosion resistance.

Several studies [8]–[13] have assessed the possibility of introducing bioactive materials within a magnesium matrix in order to produce bioactive and biodegradable composites. Among these studies, hydroxyapatite (HA) is the most common material added to the magnesium matrix since HA displays a similar composition to bone and can thereby improve the interface between the implant and the bone tissue in orthopedic applications. For example, it was shown that the incorporation of 10 wt.% of HA enhances bioactivity in an Mg-1% Ca alloy [14]. Nevertheless, it is recognized that the incorporation of a ceramic phase within a magnesium matrix may affect both the mechanical properties such as ductility and also the corrosion resistance.

The processing operations required to produce a magnesium-hydroxyapatite composite usually require at least one step at high temperature. However, it was shown recently that processing by high-pressure torsion (HPT), where there is the application of

both a high pressure and concurrent torsional straining, can fully consolidate mixed particles of both materials to produce a solid composite at room temperature without the need for any processing at elevated temperatures [15]. For example, it was demonstrated that an Mg-5% HA composite processed by HPT displays a continuous Mg matrix with well-dispersed particles of HA and the composite exhibits enhanced hardness and a tensile strength which is comparable to pure Mg [15]. Preliminary testing also revealed no toxicity in this composite and initial corrosion tests gave a low impedance and with a decreasing corrosion rate with increasing immersion time.

These earlier results provide important information on the potential for fabricating this composite without incorporating any high temperature sintering or extrusion in the processing procedure. Accordingly, the present investigation was initiated to follow this earlier study by providing a deeper characterization of the corrosion behavior of an Mg-5% HA composite with specific emphasis on the nature of the corrosion product layer which is formed after long immersion times.

2. Experimental material and procedures

For the fabrication of the HPT composite, magnesium particles (commercial purity, >99.5%) and hydroxyapatite powder (Sigma Aldrich) were hand-mixed and compacted in a hydraulic press in the proportion of 95 wt.% Mg and 5 wt.% hydroxyapatite. These compacted discs, of 10 mm diameter and ~1 mm thickness, were processed by HPT at room temperature for 50 revolutions at 6.0 GPa pressure and a rotation rate of 1 rpm. Further details of processing the composite and images of the starting materials are available elsewhere [15]. For comparison, bulk pure Mg was also processed by HPT from the as-cast condition. Samples in the shape of Mg discs with 10 mm diameter and 0.85 mm thickness were processed by 10 turns of HPT using a similar pressure and

rotation rate. The temperature rise in the course of HPT processing is estimated as ~13 K, considering a flow stress of 250 MPa [16][17][18]. Further details, including characterization before and after HPT processing, are also available elsewhere [4][19][20]

The corrosion tests were performed in triplicate at room temperature. Samples were polished with 1200 and 4000 mesh silicon carbide papers in order to remove any surface oxide layer. After sanding, samples were cleaned with alcohol and air-jet dried. The area analyzed in the tests of each sample was 0.196 cm^2. A potentiostat (Galvanostat Metrohm Autolab PGSTAT 100N) with FRA32M impedance modulus, coupled to a microcomputer with NOVA 2.1® software, was used to perform the electrochemical tests and data acquisition. A conventional electrochemical cell was used with three electrodes: an Ag/AgCl reference electrode (saturated), a platinum auxiliary electrode (Pt) and a working electrode (sample of the study material). The electrolyte used was Hank's solution produced with analytical grade reagents and distilled water according to the composition shown in Table 1. The pH was adjusted with hydrochloric acid to the range of 7.2 ± 0.1.

The Open Circuit Potential (OCP) was measured up to stabilization for 3600 seconds for the pure Mg sample and for 900 seconds for the Mg-HA composite. Thus, anodic potentiodynamic polarization tests were performed after 1 hour of immersion for pure Mg and after 15 min for the composite. The test started from the 200 mV potential below the corrosion potential at a scan rate of 1 mV s^{-1} and continued until the anodic current density reached 10^{-2} A cm^{-2}. Multiple electrochemical impedance spectroscopy (EIS) tests were performed after immersion times varying from 15 minutes to 36 hours for both materials. The tests were carried out at frequencies varying from 10^4 Hz to 1 mHz and an amplitude of 0.01 V.

Hydrogen evolution tests were performed using HPT-processed discs immersed in Hank's solution which was maintained at a temperature of 37.1°C through a thermal bath. An inverted funnel was placed over the sample and directed the bubbles of hydrogen formed on the sample surface to a test tube where it was possible to measure the volume of hydrogen collected. The volume of released hydrogen was measured at different time intervals and the rate of degradation was deduced based on the following equation:

$$Mg_{(s)} + 2H_2O_{(l)} \rightarrow Mg(OH)_{2(s)} + H_{2(g)} \quad (1)$$

Thus, it is considered that each mol of hydrogen gas is associated with 1 mole of magnesium consumed. The estimated mass loss of magnesium is therefore determined from the relationship:

$$m_{Mg} = \frac{PV_{H_2}}{RT} \times M_{Mg} \quad (2)$$

where m_{Mg} is the mass of oxidized magnesium, P is the pressure of the released gas, V_{H2} is the volume of hydrogen released during the reaction, R is the universal gas constant, T is the absolute temperature of the system and M_{Mg} is the molar mass of magnesium.

The degradation rate (DR) was calculated using the expression:

$$DR = \frac{m_{Mg}}{At} \quad (3)$$

where A is the sample total surface area and t is the time of exposure in Hank's solution. At the end of the test, the samples were washed with alcohol, air-jet dried and conditioned at an appropriate location for further characterization.

X-ray diffraction (XRD) analysis was performed before and after 60 hours of immersion in the solution. The diffractograms were collected using a Panalytical diffractometer equipped with a copper (Cu) X-ray tube operating at 45 kV voltage and 45 mA current. The scan rate was 0.02° s^{-1} in the range of 2θ between 3.00° and 119.99°.

For the study of the microstructure, morphology and composition of the corrosion product layer, scanning electron microscopy (SEM) and energy dispersive spectroscopy (EDS) were used. The equipment used was a JEOL 6360LV SEM operating at 15 kV. Metallographic techniques were undertaken to prepare a polished surface on the Mg-HA composite and evaluate the distribution of phases. Also, samples subjected to immersion in Hank's solution were dried and observed without any other preparation.

A focused ion beam (FIB) was used to cut a hole on the corroded surface of a sample of the Mg-HA composite after immersion in Hank's solution for 1 hour and this allowed observation of the corrosion product layer and substrate. FIB was used also to produce a transparent lamella. Care was taken to preserve the corrosion product layer and this lamella was observed using a Tecnai G2-20 - SuperTwin FEI transmission electron microscope (TEM) operating at 200 kV.

3. Experimental results

3.1. Characterization of the composite

The SEM image and EDS maps shown in Fig. 1a reveal a magnesium matrix with regions containing calcium and phosphorus which are elements present in the chemical structure of hydroxyapatite. The particles of hydroxyapatite are well distributed in the composite. The grain structure of the magnesium matrix is revealed by the scanning transmission electron microscopy (STEM) image in Fig. 1b. The grains are ultrafine (<1 μm) and reasonably equiaxed with a measured average grain size of ~0.31 μm. This value is smaller than observed in pure magnesium processed by HPT [19]–[21]. It has been shown that the incorporation of inert particles to produce a composite using HPT consolidation leads to smaller grain sizes than those observed in pure metals [22][23][24] .

Thus, the present results show that the incorporation of hydroxyapatite particles enhances the grain refinement induced by HPT processing of pure magnesium.

3.2. Electrochemical tests

Figure 2a shows the open circuit potential (OCP) of the Mg-HA composite as a function of immersion time in Hank's solution. A curve obtained for pure magnesium processed by HPT is also shown for comparison. The OCP for Mg-HA was higher than for pure Mg in the early stage due to the presence of a chemically stable compound in the composite. The increase in the OCP values are related to the formation of corrosion products on the surface of samples which act as a barrier against corrosion. It is noted that the OCP stabilized at different times for the samples and this suggests that the development of the corrosion product layer in pure magnesium takes longer.

Representative polarization curves of the HPT-processed Mg and Mg-HA samples are shown in Fig. 2b. The Mg-HA composite exhibits a higher corrosion potential than the Mg sample due to the presence of hydroxyapatite, a chemically stable and inert compound, confirming the OCP measurements. These results indicate that the Mg-HA composite displays a different corrosion mechanism relative to the HPT-processed pure Mg. The curve for the Mg-HA composite suggests generalized corrosion with a highest corrosion current density in relation to the Mg HPT sample. However, as the potential increases above -1.35 V the composite sample showed lower anodic currents. The HPT-processed Mg sample showed a passivation region with a passive current density of 1.63×10^{-5} A cm^{-2} and a breakdown potential of -1.41 V. However, at potentials higher than -1.35 V both samples exhibited anodic current densities which increased continuously.

For convenience, the average electrochemical parameters obtained in different polarization tests are summarized in Table 2. It is important to note that the values of the corrosion potential and corrosion current density observed in the Mg-HA composite agree with values reported for a magnesium alloy AZ91 in which a layer of hydroxyapatite was deposited [25].

Electrochemical impedance spectroscopy tests were performed after different immersion times for both the pure Mg and the Mg-HA composite. Figure 3 shows Nyquist plots for both samples. It is observed that the curves vary significantly with time. The impedance of the pure Mg increases with time up to 13 h and then decreases up to 36 h. The Mg-HA composite shows a tendency of decreasing up to 2 h, increasing resistance up to 21 h and then decreasing again at 36 h.

3.3. Immersion tests

In an aqueous solution, the corrosion of magnesium releases a volume of hydrogen that is directly proportional to the mass loss of this material. Thus, the evolution of hydrogen is a suitable method for the study of magnesium corrosion in Hank's solution. The mass loss calculation was carried out considering a stoichiometric ratio of 1:1 between the hydrogen gas released and the magnesium in the chemical reaction given by eq. (1) [26].

The calculated mass loss rates for magnesium and the composite are shown in Figure 4. Both materials display a high mass loss rate in the first hours followed by a sharp decrease and stabilization at a negligible rate. The peak of mass loss occurs firstly for the HPT-processed Mg within the first hour of immersion and then occurs after 4 h for the HPT-processed Mg-HA. The reduction of mass loss at a non-quantifiable level by the experimental setup occurred after 9 h for Mg and after 14 h for the Mg-HA composite.

It is important to note that, although there was no increase in the volume of hydrogen in the test tube after stabilization indicating that there was apparently no corrosion of the magnesium alloy, gas bubbles were identified in the environment. It was concluded, therefore, that during stabilization the mass loss was very small and the hydrogen is captured in the solution and can be released outside the measuring device.

The corroded surfaces of samples were observed in SEM after different immersion times. Figure 5a shows SEM micrographs of the Mg sample surface after immersions of 5 and 10 h. It is apparent that localized corrosion takes place with a slow increase in the volume of the corrosion product at these locations. Most of the surface shows no evidence of significant corrosion at this stage. An earlier report provided a detailed characterization of the corrosion in Hank's solution of pure Mg processed by HPT and it was shown that there is no severe localized corrosion in this material even after long immersion times [3].

Figure 5b shows SEM images of the surface of a sample of Mg-HA at different immersion times up to 60 h. The same sample was used in this investigation and it was possible to track the same location at the different times. This sample also showed evidence of localized corrosion but it is apparent that the whole surface displays the formation of a corrosion product layer. Two areas that appear to undergo localized corrosion after 5 h of immersion were also tracked at higher magnifications. The images on the left show an area that displayed deep and thin holes in the corrosion product layer after 5 h and the images on the right show an area that displayed a shallow and large hole in the corrosion product layer. The latter is evident by the grinding lines of the original surface which are clearly observed inside the hole. Both of these areas are covered by corrosion products after 10 h. The area depicted on the left shows evidence of a hole in the corrosion product layer after 36 h of immersion and it is covered again after 60 h. This suggests that localized corrosion does not propagate significantly in the Mg-HA

composite and a thick layer of corrosion product is formed which can protect these areas. The protective corrosion product layer may detach leading to the formation of a new layer. It is also observed that the whole surface of the sample displays a thick layer of corrosion products after 60 h of immersion in Hank's solution.

3.4. Characterization of the corrosion product layer

X-ray diffraction patterns for the pure Mg and the Mg-HA composite before and after immersion in Hank's solution are shown in Fig. 6a. All samples display Mg characteristic peaks in both conditions. It is interesting to note that the XRD pattern of pure magnesium shows no additional peak after immersion in Hank's solution which suggests that the corrosion product layer is too thin and the volume of material is not sufficient to appear in XRD and/or it is amorphous. The Mg-HA composite displays minor peaks of HA before immersion and the intensity of these peaks decreases after immersion which demonstrates that the corrosion product layer covers the surface.

Figure 6b shows a high magnification image of the surface of the Mg-HA composite after 5 h of immersion in Hank's solution. Corrosion products are clearly visible and cover the whole surface despite the short immersion time. However, it is apparent that the corrosion product layer is not very dense. EDS mapping of this area revealed the presence of O, Mg, P and Ca.

In order to evaluate the corrosion product layer in more detail, an FIB technique was used to make a small hole on the sample surface. Figure 7 shows SEM images of the surface (a) before and (b) after the cut. The surface was completely covered by corrosion products which display long continuous cracks. In addition, the corrosion product layer is ~2 µm thick and several small (<1 µm) pores are clearly visible. It is observed at a

higher magnification in Fig. 7c where a small crack, visible on the corroded surface, fails to propagate to the metallic substrate. The tip of this crack is denoted by an arrow.

EDS mapping was used to evaluate the composition of the corrosion product layer and the substrate. Figure 7d shows an SEM image and the distribution of Ca, P and Mg. It is observed that the surface corrosion layer is rich in Ca and P but not in Mg. A particle of hydroxyapatite is visible in the bottom left side of the image and it appears as a dense region on the SEM image which is rich in Ca and P. The magnesium substrate is visible as pockets on the left and the right sides of the image. However, careful inspection shows there is a small continuous distribution of Mg between these pockets and on the top of the hydroxyapatite particle. It is important to note that the secondary electrons (SE) image clearly shows a continuous bright phase from the corrosion product layer to the hydroxyapatite particle but the EDS mapping shows a discontinuity in the distribution of Ca and P. This region is highlighted in the images and displays a significant concentration of Mg in the EDS map. This shows that the corrosion product layer does not display a continuous composition. A layer which is rich in Ca and P and without Mg is observed at the surface and a layer rich in Mg without Ca and P is observed near the magnesium substrate.

The distribution of elements on the surface layer was further investigated using electron energy loss spectroscopy (EELS) in a TEM. Figure 8 shows a TEM image of a lamella extracted from the corroded surface of the Mg-HA composite after immersion in Hank's solution for 5 h. The corrosion surface layer is at the bottom of the image. It is noted that, during the lamella preparation, a portion of the corrosion product layer detached from the substrate. EELS point analysis was performed in 4 different locations as shown: thus, 1 is in the Mg substrate and far from the corrosion surface, 2 is in the interface between the Mg substrate and the corrosion surface, 3 is in the corrosion product

layer near the interface with Mg and 4 is in the corrosion product layer far from the interface. The portions of the EELS profiles which indicate the presence of an element are depicted and associated with the position number for that profile. As expected, only Mg was identified in position 1. However, Mg and O were identified in position 2 and position 3 contains C, K, O and Mg. It is interesting to note that C, K, Ca and O were identified in position 4 but Mg was not identified in this location. This agrees with the EDS mapping presented in Fig. 7d which showed no Mg on the external surface of the corrosion product layer. Although P was not identified in EELS, this does not mean necessarily that this element is not present since the identification of P using EELS is difficult.

The structure of the corrosion product was also investigated using electron diffraction. Figure 9 shows a TEM image and locations where selected area electron diffraction (SAED) patterns were obtained. The pattern taken on the corrosion product layer shows continuous rings which suggests an amorphous structure in this region or a nanocrystalline structure. The patterns taken on the interface and on the substrate clearly show spots associated with the Mg crystalline structure, but it was not possible to identify any other crystalline structure in these patterns.

Further investigation was carried out using high resolution TEM images. Figure 10a shows an HRTEM image near the interface between the Mg matrix and the corrosion product layer. The Mg matrix is located at the top of the image and the fast Fourier transform (FFT) image shows spots associated with the (100) planes of Mg. The whole top area of the image presents the same pattern indicating that it is the same Mg grain. The bottom of this image showed no pattern of a crystalline structure and was identified as an amorphous phase. However, a thin intermediate region, which appears darker in the image, displayed multiple patterns which were associated with Mg and MgO. An FFT of

this region shows multiple spots which were associated with Mg and MgO. It is important to note that the (200) planes of MgO were identified and there is no planar spacing close to it in Mg. Figure 10b also shows an HRTEM image of a region between the Mg matrix and the amorphous phase. This image reveals many areas without any crystalline orientation but very small crystals of MgO are visible within this amorphous structure. The FFT of this image clearly shows many spots associated with the (200) planes of MgO, thereby demonstrating that there is a layer between the Mg matrix and the external corrosion product layer in which MgO nanocrystals are embedded in an amorphous structure.

4. Discussion

It was shown earlier that HPT processing is able to consolidate Mg particles with the addition of hydroxyapatite (HA) particles to produce an Mg-HA composite [27]. The present results confirm the formation of such composite and shows there are well-distributed HA particles embedded within an Mg matrix. In addition to the room temperature consolidation of this composite, HPT processing also significantly refines the grain structure of the Mg matrix and produces an ultrafine-grained structure. It has been shown that the grain refinement induced by HPT can improve the corrosion resistance of pure Mg and some Mg alloys [3]. The present results demonstrate that the incorporation of HA particles also affects the corrosion behavior of ultrafine-grained pure magnesium. However, a description of its effect is not straightforward.

Basically, it is shown that the incorporation of HA particles increases the corrosion potential of the composite. As the matrix is composed of pure magnesium, it is expected that the HA particles exhibit a higher corrosion potential and induce a galvanic cell effect. This process increases the initial corrosion current density as is observed by the evolution

of the OCP and the polarization tests. Also, EIS tests show that the resistance against corrosion of the Mg-HA composite is smaller than in pure Mg for low immersion times in Hank's solution. However, this initial detrimental effect is alleviated after long immersion times. After an initial rapid corrosion compared to pure Mg, the Mg-HA exhibits an increase in corrosion resistance as captured by EIS and a pronounced decrease in the corrosion rate as indicated by the hydrogen evolution test. This is attributed to the gradual formation of a protective corrosion product layer on the composite surface.

The SEM images showed the occurrence of localized corrosion in both the pure Mg and the Mg-HA composite in the initial stage of corrosion. However, careful tracking of the evolution of the corroded surface shows that the areas of localized corrosion fail to evolve significantly. The corrosion products cover the areas of localized corrosion and it appears that this improves the protection in these areas. Some detaching of corrosion products may take place and new products are formed. No severe localized corrosion was observed up to 60 h of immersion in Hank's solution. In fact, the whole surface of the sample gradually becomes covered by corrosion products which shows a more general type of corrosion after long immersion times. A pseudo-uniform type of corrosion has been suggested in ultrafine grained materials [28][29] and earlier reports showed essentially uniform corrosion in ultrafine-grained pure Mg [3][4]. It is interesting to note that the addition of HA fails to change this behavior despite the potential for forming galvanic cells in a composite.

Careful inspection of the polarization test curves shows that the increment in corrosion potential in the Mg-HA composite, compared to pure Mg, moved the corrosion potential to the passivation region of pure Mg. Thus, it is possible that the high corrosion current density observed in the early stage of deformation is contributing to the formation of a more protective layer on the surface. This proposal is supported by the significantly

higher impedance observed at 13 h in the composite compared to pure Mg. It is also interesting to note that the corrosion rate observed in the hydrogen evolution test also decreased after a similar immersion period in the Mg-HA composite. Thus, the initial immersion of ~10 h in Hank's solution is associated with the formation of a more protective surface layer in the composite.

The characterization of the corrosion product at the surface of the Mg-HA composite showed that it is composed of different layers. A thin layer of MgO is in contact with the Mg substrate and a layer of an amorphous phase with nanocrystals of MgO is observed near the interface with the Mg substrate. The external layer is composed of an amorphous phase which is rich in O, Ca and P and contains K and C. This external layer contains small pores (<1 μm) and external cracks. It is interesting to note that Mg was not observed in this external layer which shows that it is composed of elements which were absorbed from the solution. Although the composition of this external layer is rich in O, Ca and P, which are the main elements in hydroxyapatite, the lack of crystalline structure in the former clearly distinguishes both phases. Thus, EDS mapping showed a discontinuity between a particle of HA in the composite and the surface product layer and this discontinuous region contained Mg which is probably an MgO-rich layer. The lack of crystallinity in the corrosion products also prevented the identification of any phase using XRD.

In practice, the Mg-HA composite produced by HPT consolidation of particles at room temperature display good corrosion resistance in Hank's solution. It has been shown that this composite displays good mechanical properties and initial biocompatibility tests revealed no toxicity [15]. Despite an early fast corrosion, this composite gradually produces a protective surface layer with absorbed Ca and P which probably aids in contact with bone tissue in orthopedic applications.

5. Summary and conclusions

An Mg-5% HA composite was successfully produced using HPT for consolidation of particles of the pure materials. Ultrafine grains with an average grain size of ~0.3 μm were introduced in the Mg matrix.

The Mg-HA composite displays higher corrosion potential, higher current density and lower impedance than pure Mg after short immersion times in Hank`s solution. After ~10 h of immersion, the impedance increases and the mass loss rate decreases in the Mg-HA composite.

The increase in corrosion resistance of the Mg-HA composite is attributed to the formation of protective corrosion products. The corrosion products are composed of a thin layer of MgO, a layer of MgO within an amorphous structure and by an amorphous layer rich in Ca, P and O which is absorbed from the solution.

Acknowledgements

The authors acknowledge the Centre of Microscopy at the Universidade Federal de Minas Gerais (http://www.microscopia.ufmg.br) for providing equipment and technical support for experiments involving electron microscopy. V.F.L. acknowledges support from CNPq (grant 306291/2018-5). R.B.F. acknowledges support from CNPq (grants 302445/2018-8 and 400407/2016-7) and Serrapilheira Institute (grant Serra-1709-17750). T.G.L. acknowledges support from the European Research Council (ERC Grant Agreement No. 267464-SPDMETALS). D.L., R.B.S. and M.M.C. received research fellowships from CAPES.

References

[1] S. Kamrani, C. Fleck, *BioMetals* **2019**, *32*, 185.

[2] R.B. Figueiredo, T.G. Langdon, *Adv. Eng. Mater.* **2018**, *1801039*, 1.

[3] D.R. Lopes, C.L.P. Silva, R.B. Soares, P.H.R. Pereira, A.C. Oliveira, R.B. Figueiredo, T.G. Langdon, V.F.C. Lins, *Adv. Eng. Mater.* **2019**, *21*, 1900391.

[4] C.L.P. Silva, A.C. Oliveira, C.G.F. Costa, R.B. Figueiredo, M. de Fátima Leite, M.M. Pereira, V.F.C. Lins, T.G. Langdon, *J. Mater. Sci.* **2017**, *52*, 5992.

[5] C. Zhang, S. Guan, L. Wang, S. Zhu, L. Chang, *J. Mater. Res.* **2017**, *32*, 1061.

[6] C. Zhang, S. Guan, L. Wang, S. Zhu, J. Wang, R. Guo, *Adv. Eng. Mater.* **2017**, *19*, 1.

[7] S. V. Dobatkin, E.A. Lukyanova, N.S. Martynenko, N.Y. Anisimova, M. V. Kiselevskiy, M. V. Gorshenkov, N.Y. Yurchenko, G.I. Raab, V.S. Yusupov, N. Birbilis, G.A. Salishchev, Y.Z. Estrin, *IOP Conf. Ser. Mater. Sci. Eng.* **2017**, *194*, 0.

[8] V.K. Bommala, M.G. Krishna, C.T. Rao, *J. Magnes. Alloy.* **2019**, *7*, 72.

[9] A. Kumar Khanra, H.C. Jung, S. Hoon Yu, K. Sun Hong, K.S. Shin, *Bull. Mater. Sci.* **2010**, *33*, 43.

[10] B. Chen, K.Y. Yin, T.F. Lu, B.Y. Sun, Q. Dong, J.X. Zheng, C. Lu, Z.C. Li, *J. Mater. Sci. Technol.* **2016**, *32*, 858.

[11] B. Ratna Sunil, C. Ganapathy, T.S. Sampath Kumar, U. Chakkingal, *J. Mech. Behav. Biomed. Mater.* **2014**, *40*, 178.

[12] R.. Campo, B. Savoini, A. Muñoz, M.A. Monge, G. Garcés, *J. Mech. Behav. Biomed. Mater.* **2014**, *39*, 238.

[13] F. Witte, F. Feyerabend, P. Maier, J. Fischer, M. Störmer, C. Blawert, W. Dietzel, N. Hort, *Biomaterials* **2007**, *28*, 2163.

[14] P.N. Lim, R.N. Lam, Y.F. Zheng, E.S. Thian, *Mater. Lett.* **2016**, *172*, 193.

[15] M.M. Castro, D.R. Lopes, R.B. Soares, D.M.M. dos Santos, E.H.M. Nunes, V.F.C. Lins, P.H.R. Pereira, A. Isaac, T.G. Langdon, R.B. Figueiredo, *Materials (Basel).* **2019**, *12*, 2609.

[16] P.H.R. Pereira, R.B. Figueiredo, Y. Huang, P.R. Cetlin, T.G. Langdon, *Mater. Sci. Eng. A* **2014**, *593*, 185.

[17] R.B. Figueiredo, P.H.R. Pereira, M.T.P. Aguilar, P.R. Cetlin, T.G. Langdon, *Acta Mater.* **2012**, *60*.

[18] K. Edalati, Y. Hashiguchi, P.H.R. Pereira, Z. Horita, T.G. Langdon, *Mater. Sci. Eng. A* **2018**, *714*.

[19] R.B. Figueiredo, S. Sabbaghianrad, A. Giwa, J.R. Greer, T.G. Langdon, *Acta Mater.* **2017**, *122*, 322.

[20] C.L.P. Silva, R.B. Soares, P.H.R. Pereira, R.B. Figueiredo, V.F.C. Lins, T.G. Langdon, *Adv. Eng. Mater.* **2018**, *21*, 1801081.

[21] K. Edalati, A. Yamamoto, Z. Horita, T. Ishihara, *Scr. Mater.* **2011**, *64*, 880.

[22] A. Bachmaier, A. Hohenwarter, R. Pippan, *Scr. Mater.* **2009**, *61*, 1016.

[23] T. Tokunaga, K. Kaneko, Z. Horita, *Mater. Sci. Eng. A* **2008**, *490*, 300.

[24] H. Asgharzadeh, H. Faraghi, H.S. Kim, *Acta Metall. Sin. (English Lett.* **2017**, *30*, 973.

[25] H.L. Yao, X.Z. Hu, H.T. Wang, Q.Y. Chen, X.B. Bai, M.X. Zhang, G.C. Ji, *J. Therm. Spray Technol.* **2019**, *28*, 495.

[26] B.A. Atrens, G. Song, M. Liu, Z. Shi, F. Cao, M.S. Dargusch, *Adv. Eng. Mater.* **2015**, *17*, 400.

[27] M. Castro, P.H. Pereira, R. Figueiredo, T. Langdon, *Lett. Mater.* **2019**, *9*, 541.

[28] H. Miyamoto, *Mater. Trans.* **2016**, *57*, 559.

[29] H. Miyamoto, M. Yuasa, M. Rifai, H. Fujiwara, *Mater. Trans.* **2019**, *60*, 1243.

Table 1 – Chemical composition of Hank's solution.

Component	Concentration (g/L)
NaCl	8.000
KCl	0.400
$MgSO_4$	0.029
$CaCl_2.2H_2O$	0.185
Na_2HPO_4	0.048
KH_2PO_4	0.060
Glucose	0.100
$NaHCO_3$	0.350

Table 2 – Electrochemical parameters obtained from polarization curves of Mg and MgHA, in Hank's solution.

Parameters	**Mg**	**MgHA**
Corrosion potential ($V_{(Ag/AgCl)}$)	-1.58 ± 0.01	-1.43 ± 0.04
Corrosion current density ($\mu A.cm^{-2}$)	5.23 ± 1.3	58.2 ± 2.1
Breakdown potential ($V_{(Ag/AgCl)}$)	-1.41 ± 0.02	---
Passive current density ($\mu A.cm^{-2}$)	16.3 ± 0.03	

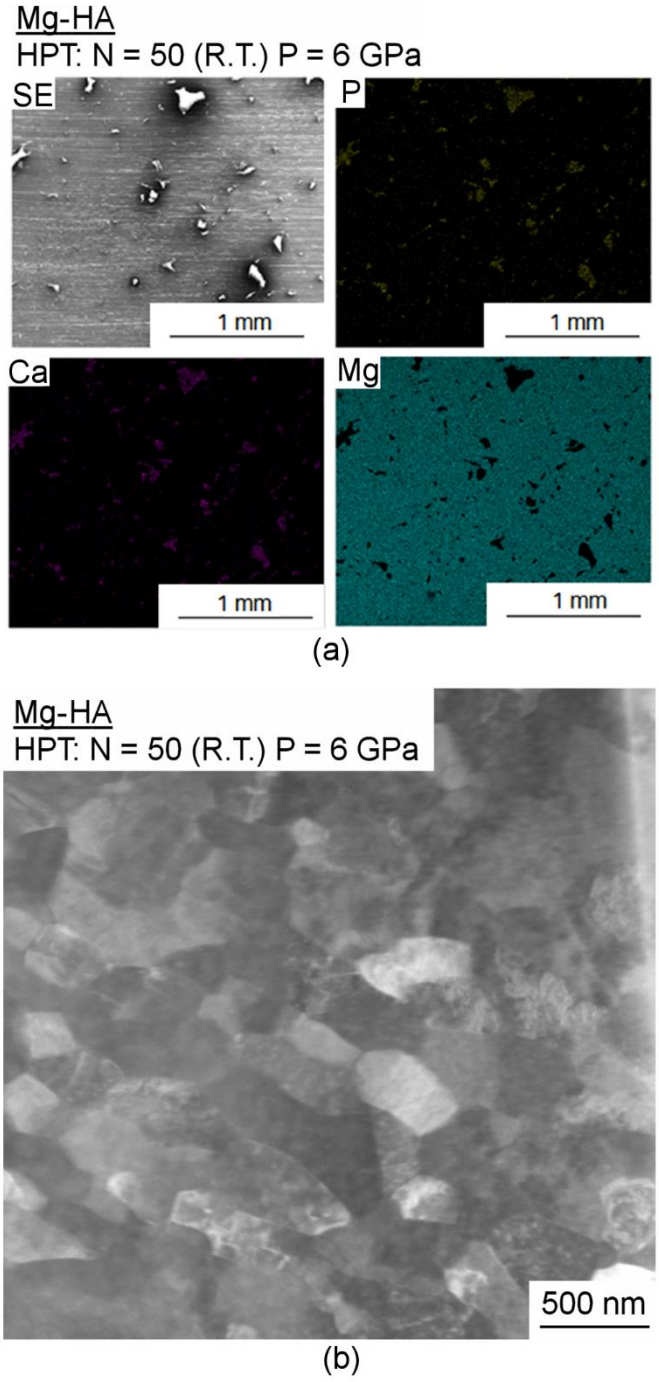

Figure 1 – (a) SEM image and EDS mapping of surface and (b) STEM image of the grain structure of HPT processed Mg-HA composite

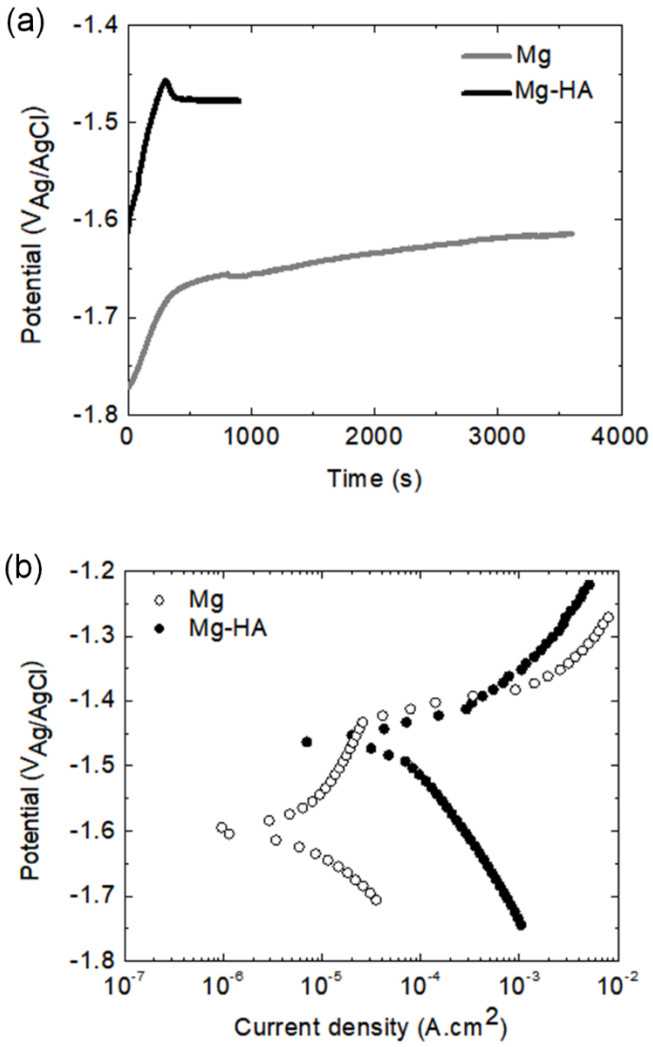

Figure 2 – (a) OCP values and (b) potentiodynamic polarization curves of HPT processed Mg and Mg-HA composite.

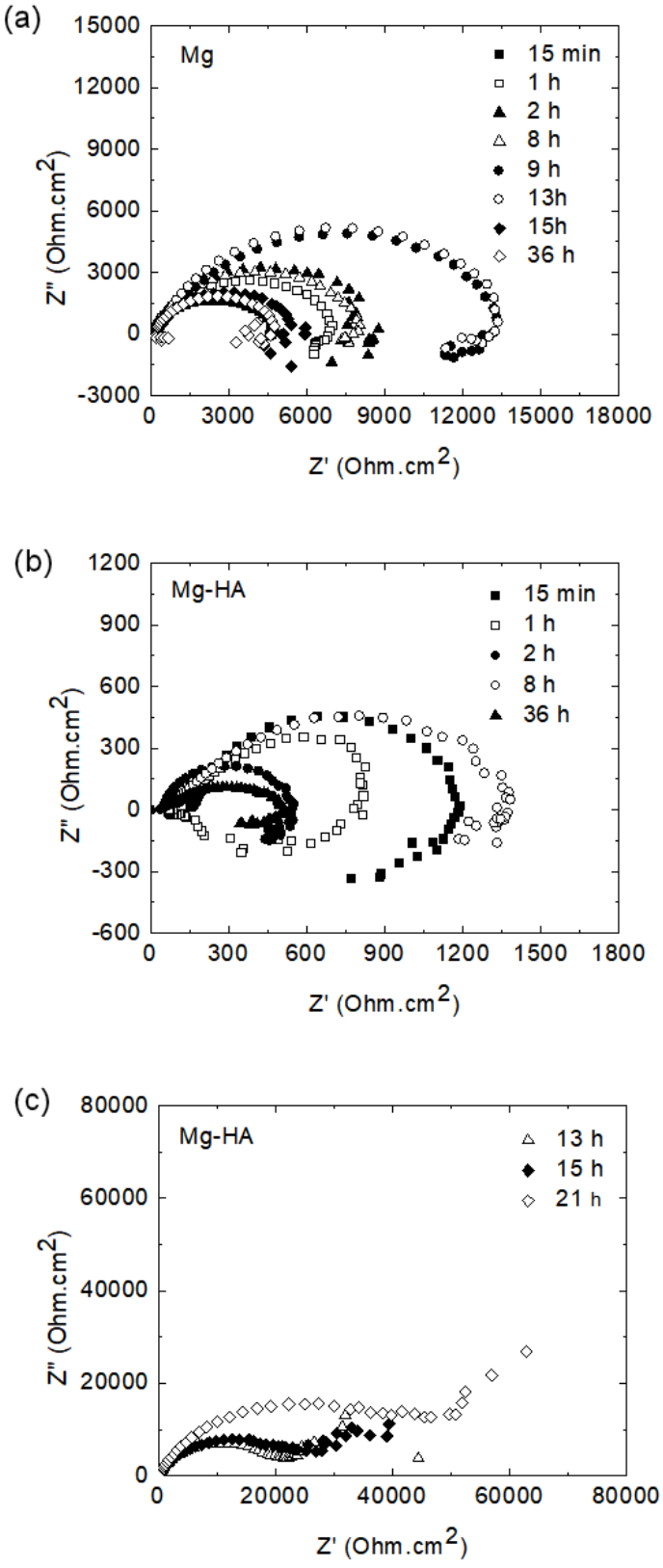

Figure 3 - Nyquist plots in for (a) Mg and (b,c) Mg-HA composite.

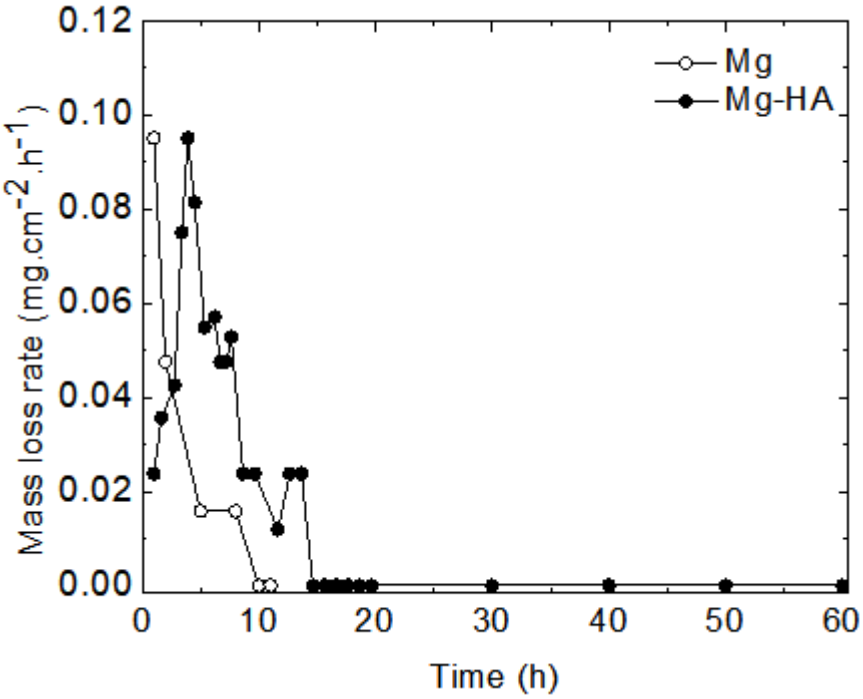

Figure 4 – Mass loss of Mg-HA and Mg processed by HPT obtained by hydrogen evolution.

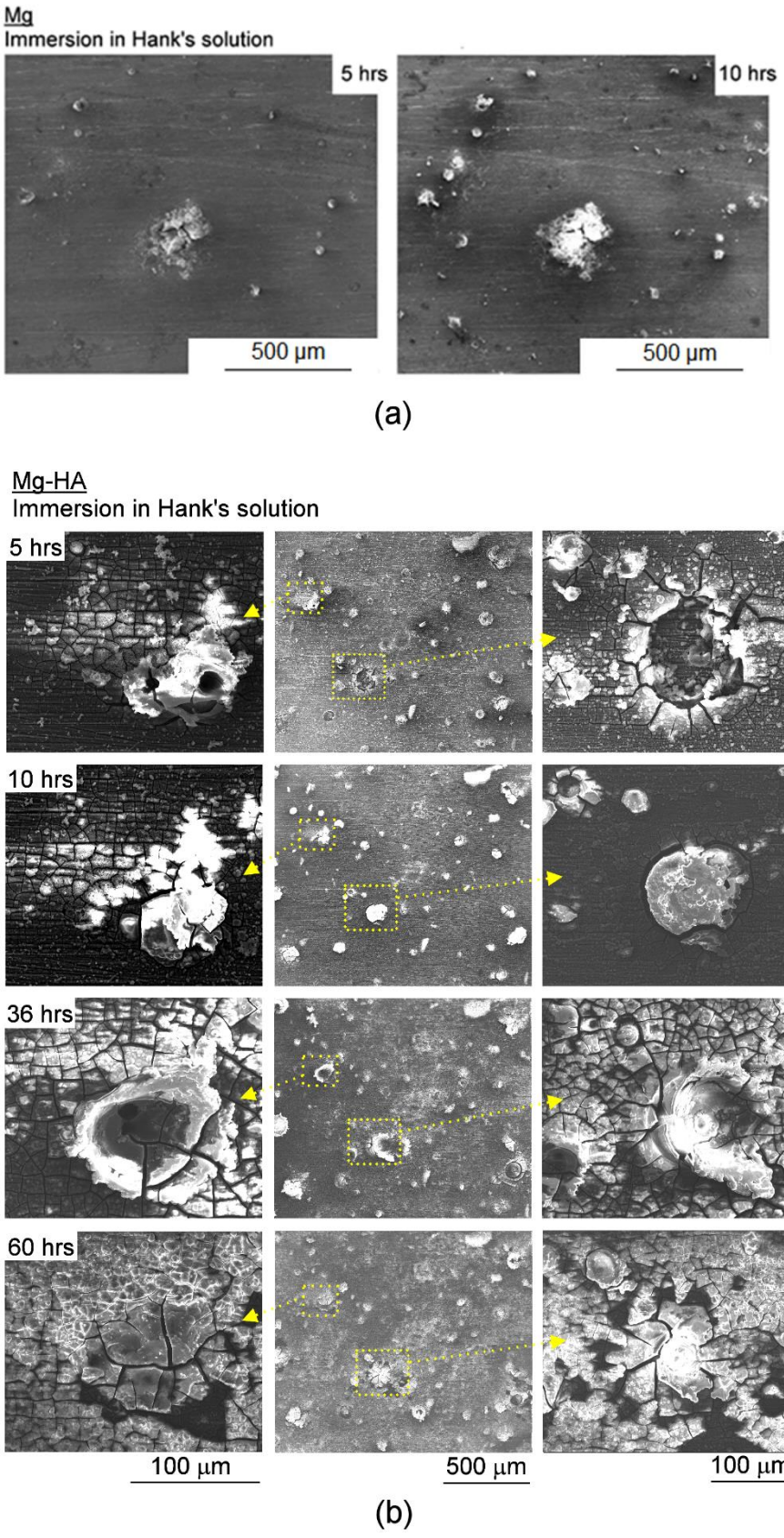

Figure 5 - (a) Mg and (b) Mg-HA surfaces after immersion in Hank's solution.

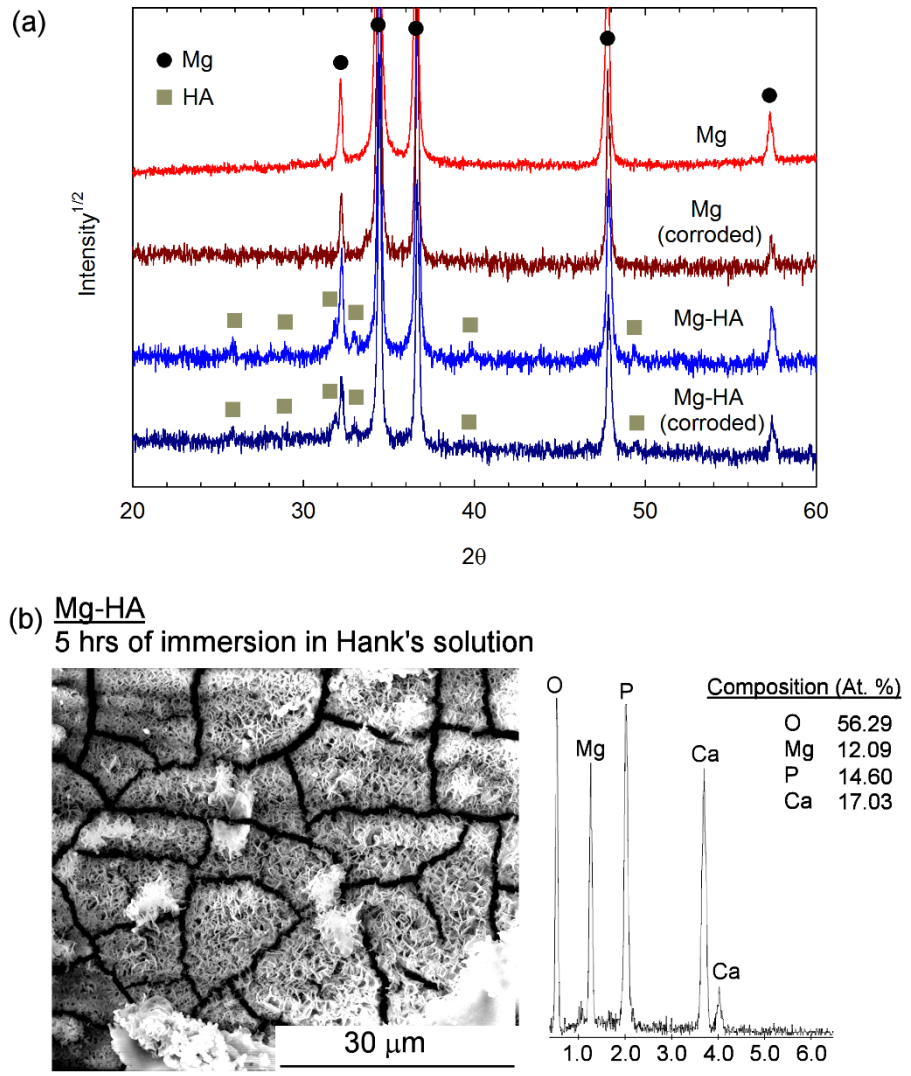

Figure 6 – (a) XRD patterns of HPT processed Mg and Mg-HA before and after immersion in Hanks solution and (b) surface features in the Mg-HA composite after immersion.

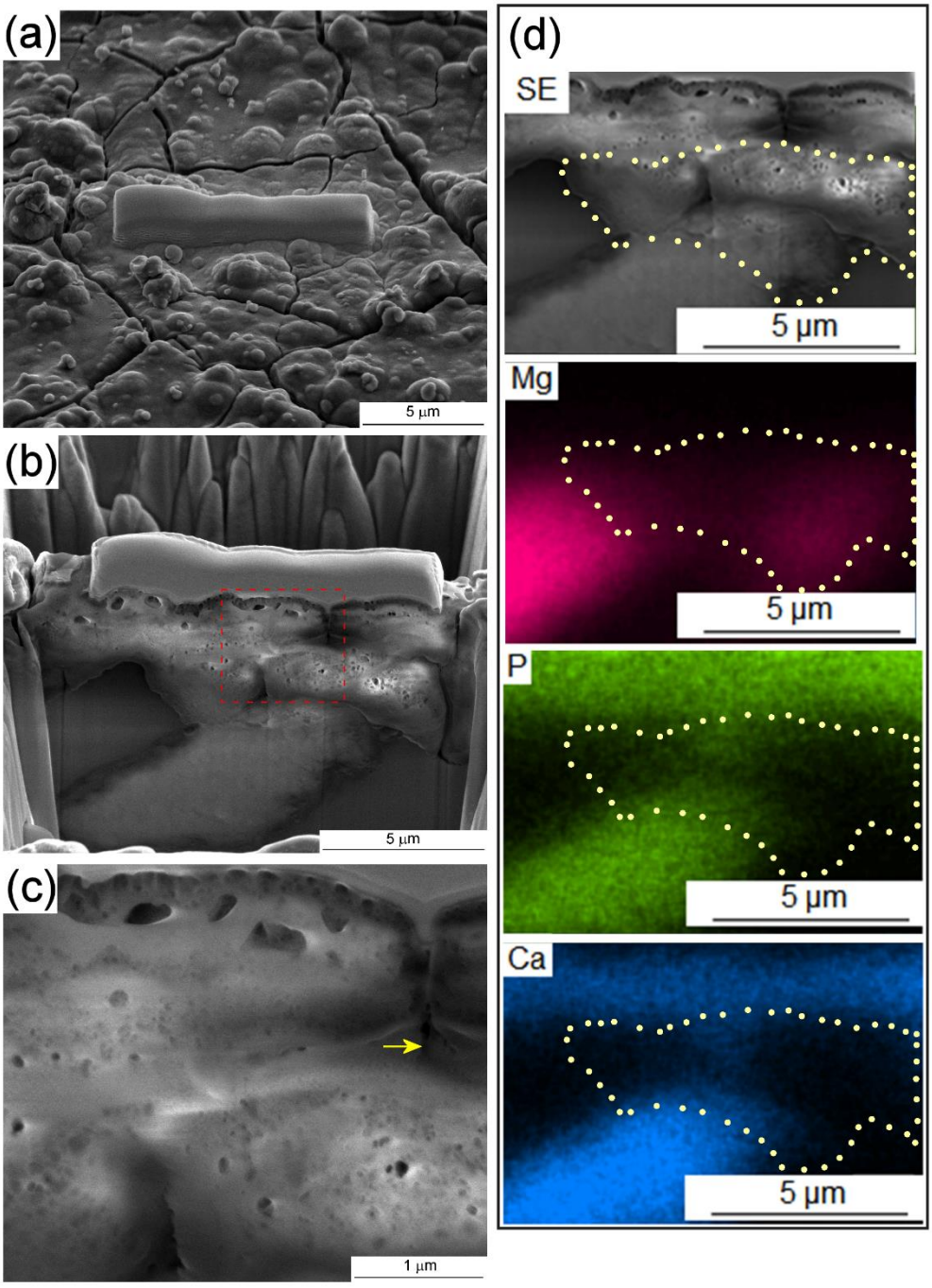

Figure 7 – (a-c) SEM images and (d) EDS mapping of a section on the surface of the sample of Mg-HA composite after immersion in Hank's solution for 5 hours.

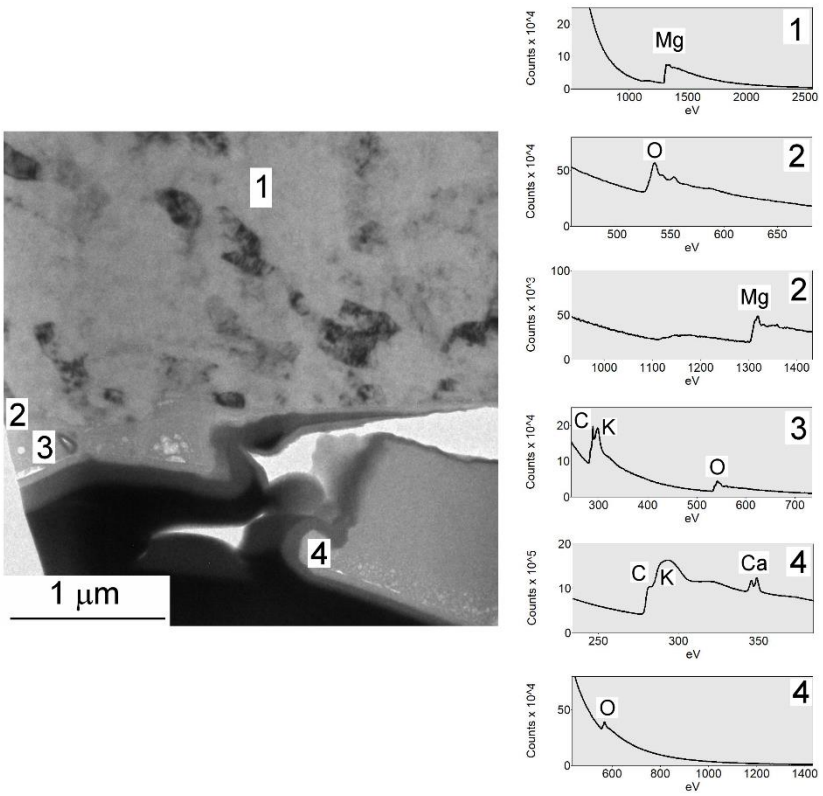

Figure 8 – EELS patterns for different locations in a TEM lamella.

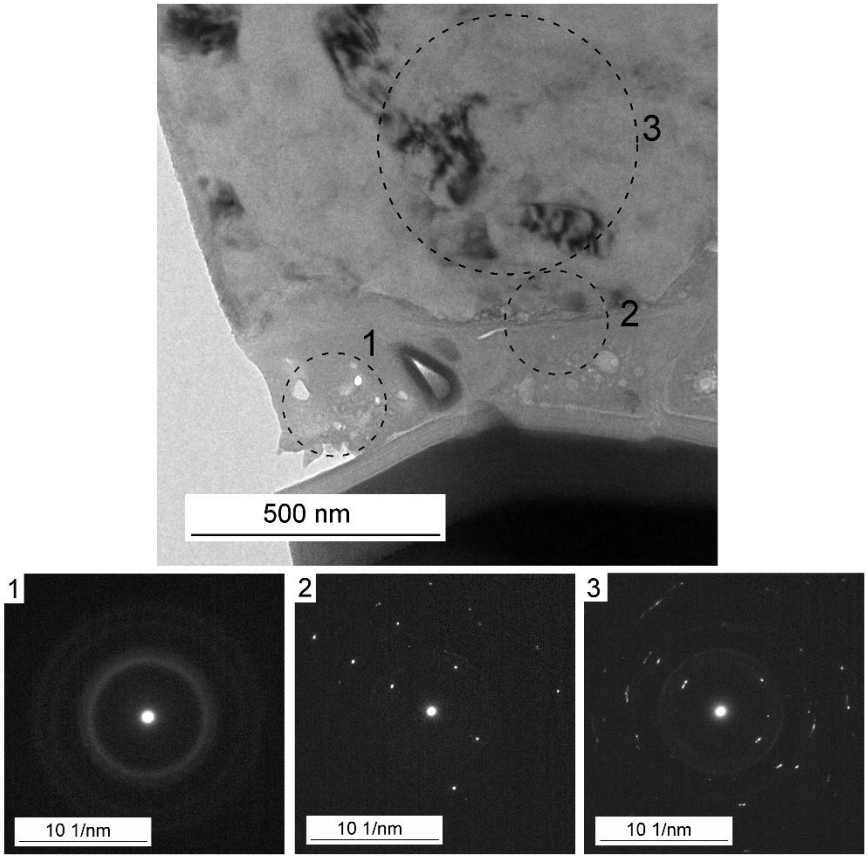

Figure 9 – SAED pattern for different locations near the corrosion surface layer in the Mg-HA composite.

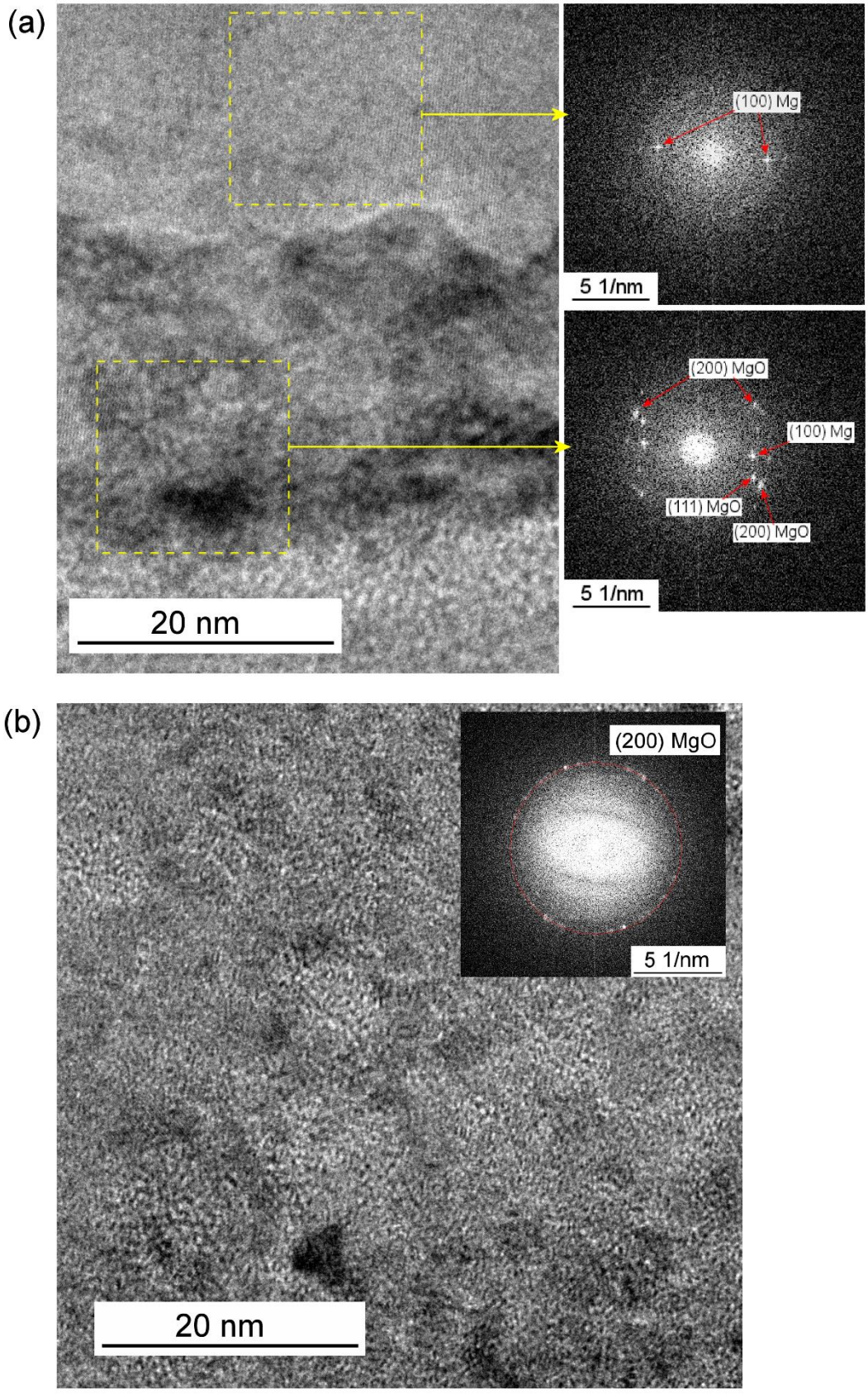

Figure 10 – HRTEM images and FFT patterns obtained near the interface between the Mg matrix and the corrosion product layer.